Astron. Astrophys. 346, 392–396 (1999)

ASTRONOMY AND ASTROPHYSICS

Dual-frequency VLBI observations of the gravitational lens system PKS 1830–211

J.C. Guirado[1], **D.L. Jones**[2], **L. Lara**[3], **J.M. Marcaide**[1], **R.A. Preston**[2], **A.P. Rao**[4], **and W.A. Sherwood**[5]

[1] Departamento de Astronomía, Universitat de València, E-46100 Burjassot, Valencia, Spain
[2] Jet Propulsion Laboratory, California Institute of Technology, Pasadena, CA 91109, USA
[3] Instituto de Astrofísica de Andalucía, CSIC, Apdo. Postal 3004, E-18080 Granada, Spain
[4] National Centre for Radio Astrophysics, Tata Institute, Pune 411007, India
[5] Max-Planck-Institut fuer Radioastronomie, D-53121 Bonn, Germany

Received 13 August 1998 / Accepted 9 March 1999

Abstract. From simultaneous 8.4 and 2.3 GHz VLBA observations we have studied the morphology and properties of the compact components of the gravitational lens PKS 1830–211. We have found that the size of the southwest component increases as λ^2, most probably due to scattering by interstellar plasma, while the size of the northeast component does not increase with such wavelength dependence. The small separation between both lensed components, compared with the typical size of scattering clumps in our Galaxy, suggests that the scattering material is located in the lensing galaxy, rather than in the Milky Way. Within the uncertainties, the flux-density ratios of the brightest feature in the two compact components for the two frequency bands agree with each other, as expected for images of the same background feature.

Key words: cosmology: gravitational lensing – galaxies: quasars: individual: PKS 1830-211

1. Introduction

PKS 1830–211 is a variable flat-spectrum radio source with two strong compact components of similar flux density separated by 1 arcsec (Rao & Subrahmanyan 1988). The unusual combination of flat-spectrum and double structure led to suggest that PKS 1830–211 was affected by gravitational lensing (Subrahmanyan et al., 1990). MERLIN and VLA observations (Jauncey et al. 1991) confirmed such suggestion by showing the similarity of the two components and, by finding the existence of an elliptical ring, interpreted as an Einstein ring, that connected them. The two components are interpreted in terms of a core-jet type source lensed by a gravitational potential.

The high flux density of PKS 1830–211 and its peculiar properties combine to make this source the target of extensive radio observations at different frequencies and resolutions. From VLA observations, the time delay between the two compact components has been estimated as 44±9 days (van Ommen et al. 1995). However a more recent result from Lovell et al. (1998) shows a time delay of 23^{+4}_{-5} days. From molecular absorption lines in the spectrum of PKS 1830-211, the redshift of a lensing galaxy has been determined as 0.89 (Wiklind & Combes 1996). Lovell et al. (1996) report the presence of a second lensing galaxy at redshift of 0.19, and suggest that PKS 1830–211 might be a compound gravitational lens. Moreover, the recent detection of the optical and infrared counterparts of PKS 1830–211 (Courbin et al. 1998; Kochanek et al. 1998), and the measurement of a redshift of 2.507 (Lidman et al. 1999) will probably allow significant improvements in the present models for this lens system (Kochanek & Narayan 1992; Nair et al. 1993), needed for an estimate of H_o. Extensive very long baseline interferometry (VLBI) observations have been carried out from cm- (Jauncey et al. 1991; Jones et al. 1993, 1996) to mm-wavelengths (Garrett et al. 1997) to monitor the morphology of the two compact components. The latter, shorter wavelength, observations show extraordinary rapid changes in the structure of the compact components that should provide strong constraints to the lens geometry.

In this paper, based on dual-frequency VLBI observations, we report the results of the analysis of the compact structures of the two main components of PKS 1830–211. From high-quality maps we have checked whether the observed angular sizes of the two images are similarly affected by interstellar scattering, and determined the flux-density ratio of the two dominant features at VLBI scales.

2. Observations and maps

We observed PKS 1830–211 on 1995 June 27 from 03:00 to 11:00 UT. Using the complete Very Long Baseline Array (VLBA), we recorded simultaneously at two frequency bands (∼8.4 and ∼2.3 GHz) in right circular polarization. The data were correlated at the National Radio Astronomy Observatory (NRAO, Socorro, New Mexico, USA) using the midpoint between the two main components of PKS 1830–211 as phase center. Manual phase calibration, visibility amplitude calibration (using system temperatures and gain curves from each antenna)

Send offprint requests to: J.C. Guirado (jcg@vlbi.uv.es)

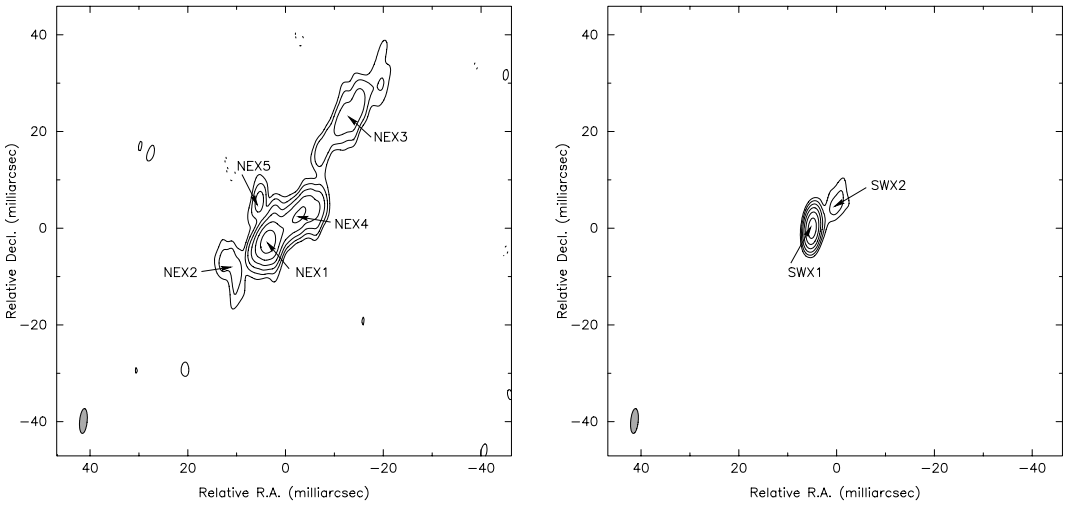

Fig. 1. Maps of the NE image (*left*) and SW image (*right*) of PKS 1830–211 at 8.4 GHz. Contours are -1,1,2,4,8,16,32,64, and 90% of the peak of brightness for each map, which is 0.57 and 1.52 Jy/beam for NE and SW image, respectively. The restoring beam (shown at the bottom left corner of each map) is an elliptical Gaussian of 5.2 mas×1.5 mas along P.A. -5.2°.

and fringe fitting at the correlation position were made with the NRAO Astronomical Image Processing System (AIPS). We transferred the data into the Caltech imaging program Difmap (Shepherd et al. 1995) to make several iterations of phase and gain self-calibration. We used a cleaning window of ∼200 milliarcseconds (mas) around the a priori positions of each of the compact components (since Difmap does not allow multiple window imaging, during the mapping process we alternately shifted the location of the window back and forth between both compact components). Therefore, at each frequency, we obtain a "global" map of PKS 1830–211 with two main features corresponding to the northeast (NE) and southwest (SW) compact components. We also mapped the PKS 1830–211 images using the task IMAGR in AIPS. Any differences of the maps obtained with Difmap and IMAGR were insignificant.

At 8.4 GHz PKS 1830–211 was detected on baselines shorter than $160\times10^6\lambda$, that is, in all baselines but those from Mauna Kea (Hawaii) to Saint Croix (Puerto Rico) and Hancock (New Hampshire). At 2.3 GHz, the source was resolved out on baselines longer than $40\times10^6\lambda$. Such interferometric performance at 2.3 GHz was expected due to the relatively low brightness temperature of PKS 1830–211, likely caused by broadening of the size of the radio images by interstellar scattering (ISS) (Jones et al. 1996; see also below).

The VLBA maps of the images of PKS 1830–211 at 8.4 and 2.3 GHz are shown in Figs. 1 and 2, respectively. At 8.4 GHz, the NE image shows a rich structure with multiple features (NEX2 to NEX5) around the strongest component NEX1; the SW image presents a one-sided core-jet structure, extending ∼10 mas towards the northwest; the emission is dominated by the unresolved component labelled as SWX1. At 2.3 GHz, the NE image shows features NES2 and NES3 around the strongest one, NES1, while the SW image shows a single extended component (SWS1).

3. Results

3.1. Separation and registration of the images at 8.4 and 2.3 GHz

To analyse the size and spectra of the compact components of PKS 1830–211 the corresponding maps at the two frequencies need to be properly aligned. At each frequency our maps contain two images, NE and SW, which are shown in Figs. 1 and 2. The separation between the images can be estimated readily from their placements in the global map. Taking the peak-of-brightness of the SW image as the origin (the choice of any other point as reference does not affect our discussion) we obtain a separation between the images of 971±2 mas along PA 48.5±0.2 and 978±7 mas along PA 48±1, at 8.4 and 2.3 GHz, respectively. The quoted standard deviations are the root-sum-square of the errors due to the signal-to-noise ratio of the map and the uncertainties in selecting and locating the delta components near the peak of brightness (quantity dominated by the uncertainty in selecting the peak of the NE component). Alternatively, the separations and uncertainties obtained from fits of elliptical Gaussian models to the visibility data are consistent with the image-based results described above. The difference between our separation estimates does not appear significant given the standard deviations. Both estimates agree with other measurements at 5 GHz (Jones et al. 1993), 22 GHz (Jones et al. 1996) and 43 GHz (Garrett et al. 1998). Accordingly, maps have been registered such that the pair of components SWX1 and SWS1, in the SW image, and NEX1 and NES1, in the NE image, coincide.

3.2. Size-broadening of the images

To obtain quantitative estimates of the flux density and size of the main components in the NE and SW images, we fitted elliptical Gaussian models to the visibility data using a least-

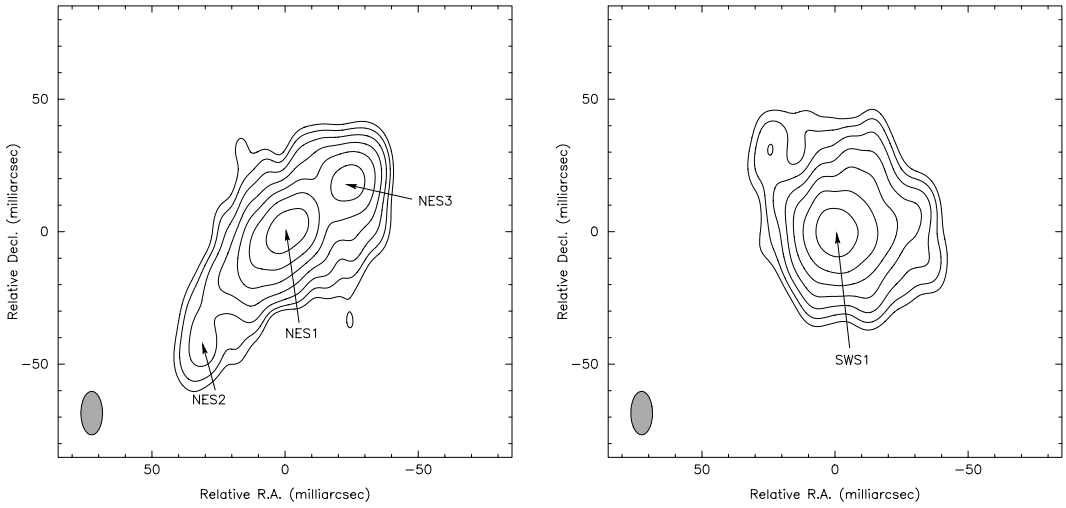

Fig. 2. Maps of the NE image (*left*) and SW image (*right*) of PKS 1830–211 at 2.3 GHz. Contours are -1,1,2,4,8,16,32,64, and 90% of the peak of brightness for each map, which is 0.56 and 0.57 Jy/beam for NE and SW image, respectively. The restoring beam (shown at the bottom left corner of each map) is an elliptical Gaussian of 16.3 mas×8.0 mas along P.A. -1.4°. Note that scales in Figs. 1 and 2 are different.

Table 1. Elliptical Gaussian models for the brightest feature in each of the NE and SW images of PKS 1830–211

λ(cm)	Component	Flux density (Jy)	Major axis (mas)	Minor axis (mas)	PA (°)
3.6	SWX1	2.0±0.2	1.5±0.2	1.2±0.2	5±9
13	SWS1	1.9±0.2	23±2	19±2	-60±20
3.6	NEX1	1.4±0.2	3.3±0.5	2.3±0.5	-70±5
13	NES1	1.2±0.2	19±3	6±3	-60±10

For each parameter, we adopt as standard deviation the increment of the (adjusted) parameter value that increases the map residuals by a factor of two.

squares algorithm. We show the most relevant parameters of the fits in Table 1, only for the brightest feature of each image. We tested whether the apparent sizes of the brightest feature increase as λ^2, as expected from broadening by interstellar scattering. From our data, we estimated the exponent β in the power law $\theta \propto \lambda^{\beta}$, where θ is the source size and λ the observing wavelength. Following Jones et al. (1996), we adopted the minor axis of each component, as given in Table 1, as the component size since this quantity is less affected by the source structure. For the SW image, our estimate $\beta = 2.1\pm0.2$ is in good agreement with the value reported by Jones et al. (1996). The use of the equivalent circular size (taken as the geometric mean of the major and minor axis) to calculate β yields a similar value. We can also estimate β by combining our size estimates with previously reported measurements of the size of the brightest feature in image SW at 1.6 GHz, 5 GHz, and 22 GHz (see Jones et al. 1996 and references therein). We then obtain (see Fig. 3) an estimate of β of 1.99±0.06. This value firmly supports the hypothesis of image SW of PKS 1830–211 being broadened by ISS.

For the NE image, assuming that the brightest peak at both frequencies corresponds to the same component, the sizes shown in Table 1 determine a value of $\beta = 0.7\pm0.5$. We also estimated β by combining our size estimates with measurements of the size of the NE image corresponding to previous observations at 5 and 22 GHz (Jones et al. 1996 and references therein). We obtain (see Fig. 3) an estimate of β of 0.65±0.15. This value is significantly different from that obtained for the SW image, which indicates a significantly smaller amount of scattering material along the line of sight towards the NE image than towards the SW image.

3.3. Flux-density ratio and spectral-index

Since gravitational lensing is a non-dispersive phenomenon, the flux-density ratio of the components of the images is expected to be independent of the observing wavelength. However, at arcsecond scales, the flux-density ratio, R, between the images NE and SW of PKS 1830–211 (in the sense NE/SW) decreases with wavelength (Subrahmanyan et al. 1990; Nair et al. 1993; van Ommen et al. 1995). This behavior of R in PKS 1830–211 is attributed to the lack of resolution of the observations to isolate, in the maps, the flux of a particular background feature (i.e. the core or a knot in the jet). Thus, at arcsecond scales, the flux density of each image is an average of the flux densities of different features, in general with different spectra and magnifications, which produces a dependence of R with wavelength. In contrast, our higher resolution and simultaneous 8.4/2.3 GHz

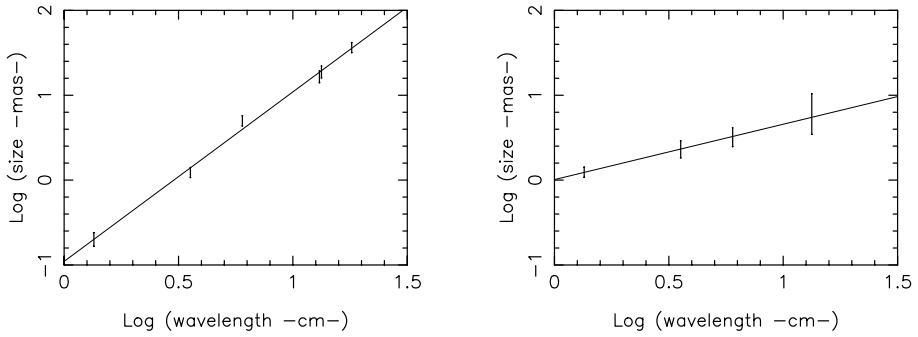

Fig. 3. Sizes of the brightest component in the SW (*left*) and NE (*right*) subimages of PKS 1830–211 at different wavelengths. For the SW image, a linear least-squares fit to the points is shown; its slope β ($\theta \propto \lambda^{\beta}$) has a value of 1.99±0.06. For the NE image, a similar fit yields a slope of 0.65±0.15. See text.

observations are suitable to test this "color invariance" property of PKS 1830–211 as a gravitational lens: components in the images of PKS 1830–211 should be less contaminated by the flux of nearby features with different spectra, and the ratio is less affected by intrinsic variability (although our observations are simultaneous at both frequencies, any rapid fluctuation of the background source seen at only one frequency in only one of the images would produce a temporal change in R). Using the flux densities in Table 1 we obtain R=0.7±0.2 and 0.6±0.2 for the brightest component at 8.4 and 2.3 GHz, respectively. This result is consistent with R being independent of frequency, as expected from gravitational images of a given background object.

The spectral indices should also be similar for both images in absence of effects other than lensing. We estimated the spectral index of the strongest components of each image from intensity maps of similar resolution (we made new 8.4 GHz intensity maps from the subset of visibility data in order to match the resolution of the 2.3 GHz intensity maps). For the NE image, the spectral index corresponding to components NEX1/NES1 is ∼0.8. For the SW image, the spectral index for the components SWX1/SWS1 is ∼1. Given the uncertainty of the registration and the different broadening due to ISS for each source, both estimates do not seem incompatible.

4. Discussion

The simultaneity of the 8.4 and 2.3 GHz VLBA images of the main components of the gravitationally lensed radio source PKS 1830–211 makes a particular contribution to the study of this source. An accurate registration of the maps at both frequencies is essential for a rigorous analysis of lens aspects. Our observations have gone some way to improve the situation but the uncertainties (2 and 7 mas at 8.4 and 2.3 GHz, respectively) are still relatively large.

From the registration adopted in Sect. 3.1, we have shown that the size of the SW image follows a λ^2–dependence ($\beta = 1.99 \pm 0.06$) while the size of the NE image does not ($\beta = 0.65 \pm 0.15$). The λ^2–scaling of the angular size of the SW image shows that it is clearly dominated by scattering caused by propagation of the wavefront through turbulent interstellar plasma (e.g. Rickett 1990).

From the different λ-dependence of the size of both components, it follows that the angular diameter of the clump of scattering material must be $<1''$. At Galactic distances, this corresponds to a clump diameter <0.04 pc, much smaller than the typical size of the clumps of scattering material in the Milky Way (1–10 pc; Cordes et al. 1984). Thus, despite the low galactic latitude of PKS 1830–211 (b=–5.°7), it is unlikely that the plasma causing the strong scattering in the SW image lies in our Galaxy. Rather, our results favor the hypothesis of the SW image being scattered by interstellar plasma in the lensing galaxy at z=0.89. The distinct scattering behaviour of the two images can be readily explained by the separation of the line of sight of both components in passing through the lensing galaxy. At z=0.89, such a separation corresponds to a distance of 5.6 kpc measured in the plane of the sky (H_0=75 km s^{-1} Mpc^{-1}, q_0=0.5). Assuming clumps of scattering material similar to those in our Galaxy, it is not unlikely that two regions in the lensing galaxy separated by such a large distance show different scattering properties. In addition, recent observations by Courbin et al. (1998) and Kochanek et al. (1998) in the optical and near-infrared show the lensing galaxy slightly closer to the SW image. Hence, the line of sight towards the SW image is passing closer to the center of the lensing galaxy than that of the NE image and, assuming a radial slope of the distribution of free electrons (similar to the distribution in the Milky Way; Taylor & Cordes 1993), through a region where scattering is stronger.

From the detection of HI absorption lines towards the line of sight of the NE image, Lovell et al. (1996) propose the existence of a second intervening galaxy at z=0.19. Our results do not indicate ISS broadening of the angular sizes of the NE image. Wiklind & Combes (1998) have not found traces of molecular absorption towards the line of sight of this image, suggesting that the alignment between the NE image and this second lens is not exact. Again, the line of sight towards the NE image would pass through areas relatively far from the center of the galaxy, where scattering is weaker.

We have found that the estimated ratio R of the flux density of the most compact features of the NE and SW images is, within uncertainties, the same for the two observing frequencies. In addition, the values of the spectral index α at the peak of brightness of the two images are also very similar. Although some differences, both in R and α, could be expected given the multiple spots around the brightest component of the NE image, the coincidence of the values is consistent with lensing. Our results suggest that NEX1(NES1) and SWX1(SWS1) are gravitational images of the same background feature. Compar-

ison of our values for R with those obtained by other authors are limited by the intrinsic variability of the source. In fact, our values of R differ significantly from those provided by Garrett et al. (1998) from observations at higher frequencies.

Our observations show a disparity of structures in both images that does not facilitate its detailed interpretation within models proposed for this lens system. Nair et al. (1993) model the compact structure of the NE(SW) image as a core and a southeast(northwest) knot in the jet. Following their model, components NEX1 and NEX2 would be gravitationally related with SWX1 and SWX2. However, the rest of the components in the images are difficult to interpret: first, extension NEX4, seen also at higher frequencies (Garrett et al. 1997), does not appear to have any correspondence in the SW image; second, component NEX3 and NEX5, which are not artifacts of our mapping, have no correspondence in the SW image either; and third, none of the 2.3 GHz features around NES1 seem to have any correspondence in the SW image in Nair et al.'s model. This striking lack of correspondence between the NE and SW images at 8.4 and 2.3 GHz is difficult to explain from time delay effects (i.e. component NEX4 is seen in maps at different epochs and frequencies (Garrett et al. 1997)). Instead, this persistent difference in the structure between the two images of PKS 1830–211 lends support to the hypothesis of the system being also lensed by a second system at z=0.19, as proposed by Lovell et al. (1996). Further monitoring of the morphology of PKS 1830–211 in time scales shorter than the estimated gravitational time delay should lead to a correct interpretation of the components in both images. Also, simultaneous observations at several frequencies should permit a more accurate checking of the dependence of the size of the NE image with the observing wavelength.

Acknowledgements. We wish to thank the referee Ian Browne for helpful suggestions which substantially improved the paper. This research has been supported in part by the Spanish DGICYT research grants PB93-0030, PB94-1274, and PB96-0782. Part of this research was performed by JCG at the Jet Propulsion Laboratory, California Institute of Technology. Research in JPL is carried out under contract with the National Aeronautics and Space Administration. The National Radio Astronomy Observatory is operated by Associated Universities Inc., under a cooperative agreement with the National Science Foundation.

References

Cordes J.M., Ananthakrishnan S., Dennison B., 1984, Nat 309, 689
Courbin F., Lidman C., Frye B.L., et al., 1998, ApJ 499, L119
Garrett M.A., Nair S., Porcas S.W., Patnaik A.R., 1997, Vistas in Astronomy 41, 281
Garrett M.A., Leppänen K., Porcas R.W., et al., 1998, In: Zensus J.A., Taylor G.B., Wrobel J.M. (eds.) IAU Colloquium 164: Radio Emission from Galactic and Extragalactic Compact Sources. ASP Conference Series Vol. 144, p. 313
Jauncey D.L., Reynolds J.E., Tzioumis A.K., et al., 1991, Nat 352, 132
Jones D.L., Jauncey D.L., Preston R.A., et al., 1993, In: Davis R.J., Booth R.S. (eds.) Sub-arcsecond Radio Astronomy. Cambridge University Press, p. 150
Jones D.L., Preston R.A., Murphy D.W., et al., 1996, ApJ 470, L23
Kochanek C.S., Narayan R., 1992, ApJ 401, 461
Kochanek C.S., Falco E.E., Impey C., et al., 1998, The CASTLES Web pages: http://cfa-www.harvard.edu/castles/ 1830.html
Lidman C., Courbin F., Meylan G., et al., 1999, ApJ, in press (astro-ph/9902317)
Lovell J.E.J., Reynolds J.E., Jauncey D.L., et al., 1996, ApJ 472, L5
Lovell J.E.J., Jauncey D.L., Reynolds J.E., et al., 1998, ApJ 508, L51
Nair S., Narasimha D., Rao A.P., et al., 1993, ApJ 407, 46
Rao A.P., Subrahmanyan R., 1988, MNRAS 231,229
Rickett B.J., 1990, ARA&A 28, 561
Shepherd M.C., Pearson T.J., Taylor G.B., 1995, BAAS 27, 903
Subrahmanyan R., Narasimha D., Rao A.P., Swarup, G., 1990, MNRAS 246, 263
Taylor J.H., Cordes J.M., 1993, ApJ 411, 674
van Ommen T.D., Jones D.L., Preston R.A., Jauncey D.L., 1995, ApJ 444, 561
Wiklind T., Combes F., 1996, Nat 379, 139
Wiklind T., Combes F., 1998, ApJ 500, 129